INTERNATIONAL JOURNAL OF TECHNO-ENGINEERING
IJTE

ISSN: 2057-5688

MACHINE LEARNING-BASED RESEARCH ON PROTON RADIOGRAPHY WITH PROTON ENERGY RESOLVED DOSE IMAGING

Adivishnu N, Research Scholar, Department of Physics , Radha Govind University, Ramgarh,Jharkhand.

Dr. Sachin Saxena ,Assistant Professor ,Supervisor, Department of Physics ,Radha Govind University, Ramgarh, Jharkhand

Abstract: Proton therapy is one of the modern cancer treatment methods with expanding demand globally. Range uncertainty, which decreases the quality of proton treatments, is a problem that hasn't yet been solved. Proton imaging newline is a possible method for reducing newline uncertainty, which is the range uncertainty that occurs from the calibration curve that converts x-ray Hounsfield newline units (HU) to relative stopping power (RSP). Proton energy resolved newline dose imaging (pERDI), a more recent technique for proton newline imaging, is based on the energy dependence of the dose newline distribution generated by a scanned proton beam. Due to the use of a single detector to assess the exit dose with varying beam strengths, this approach has the main advantage of reducing setup complexity. newline This work presents novel concepts in the cutting-edge field of proton radiography using the pERDI technology. This thesis focuses on the pERDI technique to generate proton radiographs using a number of techniques, such as the and#967;2-minimization technique, an analytical expression, and various machine learning (ML) techniques, such as neural networks from the Keras library, the Extreme Gradient Boosting (XGboost) algorithm, and advanced deep learning (DL) techniques. newline The first portion of the thesis presents the study on the newline accuracy that may be reached using the pERDI technique in homogeneous and heterogeneous newline media. The results are promising since all homogeneous inserts of tissue surrogates were measured with an RSP with a precision newline more than 1.5%, and achievable WEPL newline accuracy in a homogeneous media was within 1 mm using the Lynx detector. newline The first results demonstrated that the WEPL and RSP newlines

INTERNATIONAL JOURNAL OF TECHNO-ENGINEERING
IJTE
ISSN: 2057-5688

may be estimated with clinically acceptable precision using the newline vi newline pERDI technique.

Keywords: Proton, Energy, dose-imaging,

I Introduction

The most typical method in the pRG system is to follow the protons with many detectors while measuring the monoenergetic proton beam's range or residual energy using a calorimeter, ionisation chamber, or range telescope. This adds to the system's complexity and size, and its integration into a clinical system necessitates a different arrangement. The beam characteristics are further impacted by the placement of the several detectors. A obstacle to deployment in the clinical environment is the imaging time and expense of the full tracking system[1].

Utilising a single detector has as its primary goal to simplify the complexity of the experimental setup. E H Bentefour et al. has introduced one of the methods in this area, which produces ERDFs by using a single detector and various beam energy [2]. This method needs a calibration dataset that connects ERDFs and WEPL, which is assessed using a water phantom with predetermined size and form.

Any object's WEPL may be estimated using a pattern matching approach and the calibration dataset if you know its ERDF. The proton energy-resolved dose imaging (pERDI) technique is the name of this procedure. This method simplifies the experimental setup and may be used to scanning beam systems already present in proton treatment facilities. Additionally, the exit dosage may be recorded using the x-ray flat panels without the need for any extra setup or equipment. The findings discussed in this chapter are documented in [3].

Figure 1 depicts a pRG system with tracking detectors and a range telescope as well as the pRG method employing a single detector and a multiple beam energy system. This side-by-side picture illustrates the flexibility of a single detector system in terms of the quantity and placement of detectors.

INTERNATIONAL JOURNAL OF TECHNO-ENGINEERING
IJTE
ISSN: 2057-5688

The MCS effect results in poor quality and blurry pictures while employing proton radiography. The xCT pictures were described in chapter 3, and a variety of procedures are being investigated to provide images that are comparably superior. The pERDI methodology was used in chapter 4 to demonstrate one novel approach in this area. Although the produced pictures demonstrated acceptable RSP calculation accuracy, there is still an issue of how to deal with the range mixing effect, which is noticeable when high and low densities meet. The pERDI method is contrasted in this chapter by a different strategy. In order to estimate WEPL, a generic equation that just includes the energy and dosage from the ERDF calibration library data has to be developed. An effort is made to use an equation to connect the energy and the observed dosage to the associated WEPL rather than comparing each unique ERDF with the calibration library to determine WEPL corresponding to the minimum 2 values. The primary goals of adopting a generic formula are to validate the attainable accuracy in this methodology and to shorten the imaging time needed to obtain WEPL pictures as compared to the pERDI method.[4]

II Litreature Survey:

It has been shown that there is a strong correlation between phalangeal QUS (Quantitative Ultrasonography) values, particularly BTT (bone Transmission Time) in the proximal phalanges of the hand, and skeletal age in children and adolescents [5]. These charts will show you the presence of every carpal, as well as visible epiphyses on metacarpals and phalanxes. The radiologist will take between 2 and 3 minutes to position the probe (longitudinal, transverse, etc.) in two planes for each finger. The Greulich Pyle Atlas can be used to estimate bone age in ultrasound departments.

Therefore, in light of the aforementioned studies, we can see that researchers have evaluated the validity of ultrasound as an age estimation tool by performing ultrasonography at various anatomical sites such as the wrist, knee, calcaneus, elbow, and clavicle, and have found

INTERNATIONAL JOURNAL OF TECHNO-ENGINEERING
IJTE
ISSN: 2057-5688

encouraging prospects except for one study which concludes that ultrasonographic assessment should not yet be considered a valid replacement for radiographic bone age determination.

Schmidt and co-workers conducted a pilot study in 2011, which examined the use ultrasonography to determine the apophyseal formation of the iliac crown. According to the minimum age ranges that were developed in the context of the research, [6], there is the possibility of a reliable diagnosis being made at an age as young as 14 years. This age also applies for asylum cases.

The intra-examiner and inter-examiner agreements for the ultrasonographic assessment of Risser's Sign at the iliac crest were also confirmed to be valid in another investigation. The comparison of sonographic and radiographic Risser's stage detection in 41 participants revealed a 90.2% overall accuracy for the ultrasound test.

With its built-in benefits of accessibility, rapid scan times, multi-planar and real-time imaging, and contra-lateral comparison, ultrasonography may be used as a radiological modality that is affordable, radiation-free, and operator independent. This may be used to estimate age even in ambulatory situations. Since cartilage and tiny ossification centres may be seen with ultrasonography, it is more sensitive than radiography. For determining an infant's skeletal age, ultrasonography is a reliable substitute for traditional radiography due

The benefits of using an ultrasound instrument to determine bone age are what remain, then. Due to its objectivity and accessibility, it could be a viable alternative to traditional radiographic procedures for determining skeletal age[7].

In such situation, in addition to the clavicle and skeletal components of the hand, additional ultrasound exploration of the epiphysis of the iliac crest may provide promising prospects for determining the skeletal age in the critically essential medical and legal age range of 14 to 21 years. This is because it finished maturing rather late.

INTERNATIONAL JOURNAL OF TECHNO-ENGINEERING
IJTE
ISSN: 2057-5688

A technique was developed for evaluating the sonomorphologically-determined apophyseal maturity stage at the iliac crown in accordance with the staging established by Schulz and colleagues. [8]. Anatomical points of orientation, which may sometimes be difficult to locate by palpatory techniques as specified by Risser's stage, are now resolved since this staging is size-independent.

Therefore, the goal of the current research is to evaluate the degree of agreement between radiography and ultrasonography for estimating age at the iliac crest. We will also assess whether ultrasonography can replace radiography for age estimation in the medico-legally significant age groups of 14 to 22 years, which make up the majority of the population routinely presenting to forensic clinicians, radiologists, dentists, and all others who are concerned with age estimation exercises[9]. This evaluation will be done in the light of the results that are currently available.

The physics of proton therapy is discussed in this chapter, along with the interactions of various particles in water, the link between proton energy and range, the many treatment modalities used in proton therapy, as well as its benefits and drawbacks. Radiation therapy's primary objective in the treatment of cancer is to deliver as much energy as possible to the tumour in order to damage its DNA and halt the proliferation of uncontrolled cells while protecting nearby healthy tissues and the OAR from needless radiation[10]. Proton therapy, as the name implies, employs protons to treat tumours instead of the high-energy photons and electrons that are employed in conventional radiation treatment to treat cancer. Particles may disperse, leave energy behind, or even halt as they go through matter. The dosage, also known as the amount of energy deposited per unit mass, is determined by the kind of particle, energy, beam intensity, and density of the substance through which it passes. The tumour should get the maximal dosage possible while the surrounding tissues only receive a small amount. Numerous research are now being conducted to help accomplish this and

INTERNATIONAL JOURNAL OF TECHNO-ENGINEERING
IJTE
ISSN: 2057-5688

enhance the quality of life after therapy. [11–12].

III Methodology

Erdf theory

A monoenergetic proton beam deposits dose into a material medium when it passes through a certain depth in the medium; the remaining dose is transported as exit dose. A dose-energy sequence may now be achieved by delivering a series of monoenergetic proton beams with varying but closely spaced energies. For a certain WEPL and an energy sequence, this dose-energy connection is exclusive. Due to the proton's well defined Bragg peak [13], its peculiar character exists. The following is an explanation of the connection between dosage and energy: Consider a series of monoenergetic proton beams, designated as the "imaging field," with energies E1, E2,... En. These beams deposit doses D1, D2,... Dn in the detector, respectively, as they travel through a water medium with a thickness of w1. The dosage left behind after raving through w1 is distinct, and the pattern of dose that results as a function of energy is unique to w1. The dosage pattern is then generated by switching the water medium thickness to w2 while still employing the same imaging field. The dosage pattern derived from w2 is unique and distinct from that acquired from w1 with a shifted peak. Figure 16 presents a schematic of this configuration. As the WEPL declines, the top of the ERDF moves to the lower energy scale (left). Figure 1 displays the ERDFs corresponding to three distinct WEPLs.

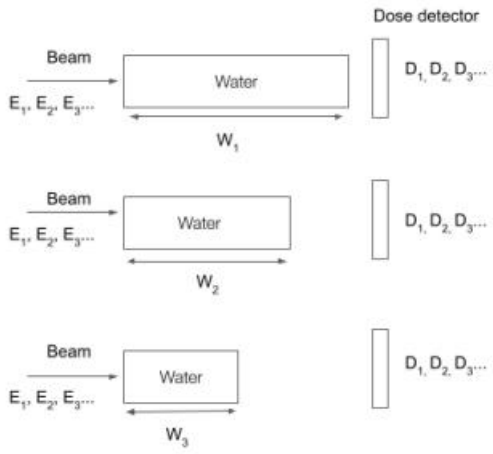

INTERNATIONAL JOURNAL OF TECHNO-ENGINEERING
IJTE
ISSN: 2057-5688

Figure 2: Schematic illustration of the configuration for producing distinct ERDFs for various water depths.

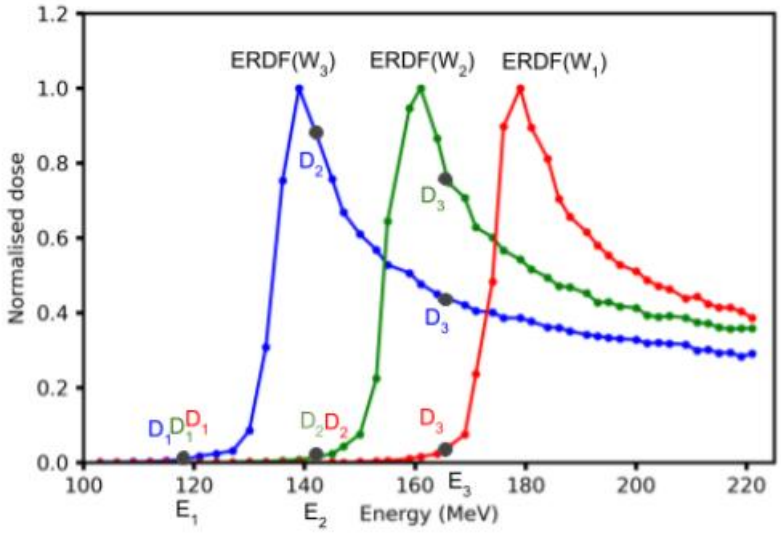

Figure 3: ERDFs from the ERDF calibration library that correspond to three distinct WEPLs.

The dose distribution from a collection of monoenergetic proton beams is often unique for a given depth of a homogeneous medium and encodes the depth of the medium traversed. The energy resolved dose function [12] is the special relationship between the dose deposited and the incoming beam energies for a certain depth. D(Ei = 1: n)|x may be used to represent this. The thickness of any object may thus be calculated by knowing its ERDF. The term "pERDI technique" refers to a method that creates 2D pictures of any object using ERDFs. This method needs a calibration dataset that connects ERDFs and WEPL, which may be calculated using water phantoms with predetermined sizes and shapes. This calibration library is regarded as the de facto reference library for obtaining WEPL for any item. Consider an object with unknown WEPL wx, for instance. Using the pattern matching approach, the ERDF corresponding to wx is compared to every other ERDF in the calibration library. For wx, the WEPL awarded

INTERNATIONAL JOURNAL OF TECHNO-ENGINEERING
IJTE
ISSN: 2057-5688

fits the ERDF the best and corresponds to it.

Steps for calibrating

The calibration library, which serves as a guide to estimate WEPL for the other three specified configurations, is made using a wedge-shaped geometry. The wedge's dimensions allow for an estimation of the WEPL for each pixel along the beam path. The first estimate is the average dosage in the pixels that are a part of the regions with the same WEPL. The ERDF is created by adding the dosage for each energy layer that was consumed. The observed ERDF curves for WEPL 71 mm are only partially complete due to partial covering of the Bragg peak. As a result, the research does not take into account the erroneous calculation of WEPL from such curves. Figure 7 depicts the process for obtaining the calibration ERDF database.

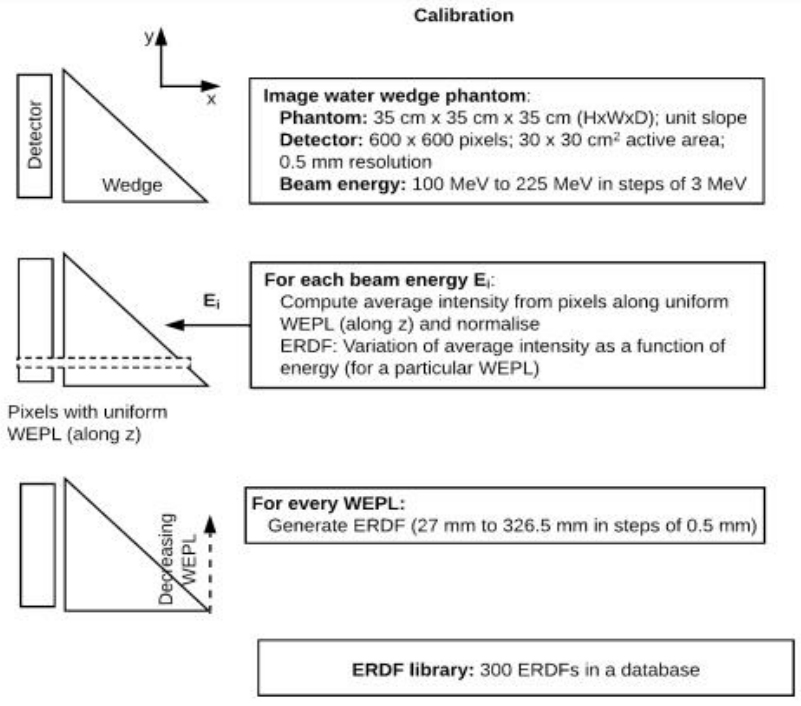

Figure 7 : Workflow to create the calibration library [7].

Imaging procedures

Making pixel-wise ERDFs from the measured data and comparing them to the calibration library are phases in the

INTERNATIONAL JOURNAL OF TECHNO-ENGINEERING
IJTE
ISSN: 2057-5688

process of creating the WEPL picture for all the configurations utilised. The ERDF of a particular pixel is computed using the pixel values received from the image field that was used during the experiment. The best matching ERDF will be found using the two-minimisation technique described above, once libraries made by the water wedge. Each ERDF from the calibration database has a WEPL that is specific to it. Figure 8 depicts the creation of the WEPL Map.

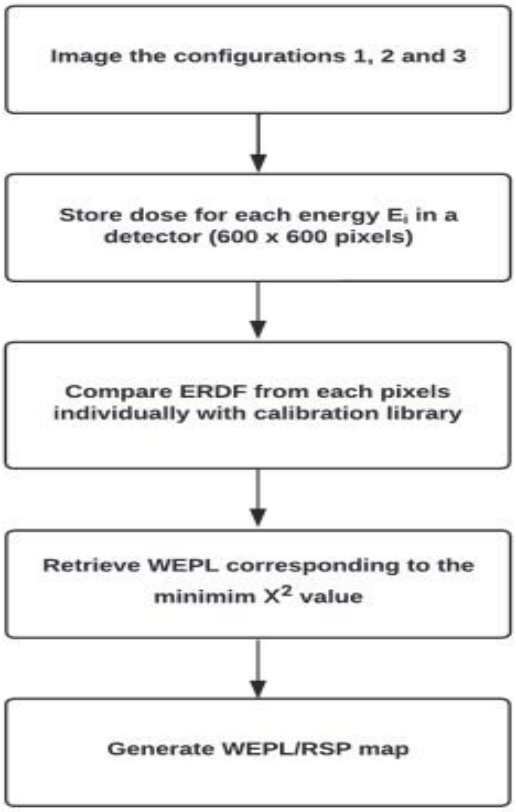

Figure 8.: Steps to calculate the WEPL picture from the ERDF library

IV Experiments and Results

The MCS effect results in poor quality and blurry pictures while employing proton radiography. The xCT pictures were described in chapter 3, and a variety of procedures are being investigated to provide images that are comparably superior. The pERDI methodology was used in chapter 4 to demonstrate one novel approach in this area. Although the produced pictures

INTERNATIONAL JOURNAL OF TECHNO-ENGINEERING
IJTE
ISSN: 2057-5688

demonstrated acceptable RSP calculation accuracy, there is still an issue of how to deal with the range mixing effect, which is noticeable when high and low densities meet. The pERDI method is contrasted in this chapter by a different strategy. In order to estimate WEPL, a generic equation that just includes the energy and dosage from the ERDF calibration library data has to be developed. An effort is made to use an equation to connect the energy and the observed dosage to the associated WEPL rather than comparing each unique ERDF with the calibration library to determine WEPL corresponding to the minimum 2 values. The primary goals of adopting a generic formula are to validate the attainable accuracy in this methodology and to shorten the imaging time needed to obtain WEPL pictures as compared to the pERDI method.

The relationship between the area under the curve and the related WEPL is thus feasible at this point.

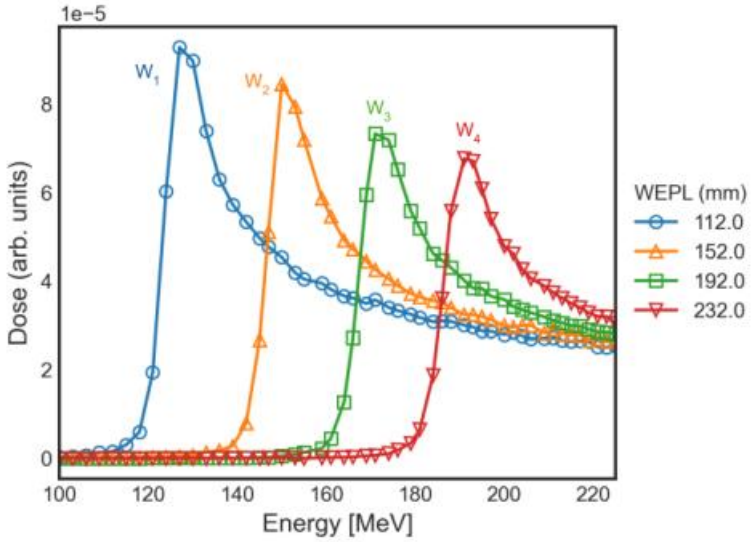

Figure 9 shows how the ERDFs in the calibration library match to four distinct WEPLs.

The dosage deposited in a material also relies on the strength of the proton beams utilised, it should be mentioned. Depending on the beam intensity, the peak and distal edge heights vary considerably. Figure 5.3 illustrates this impact with two different beam intensity. Different ERDFs for the same WEPL are caused by the impact

INTERNATIONAL JOURNAL OF TECHNO-ENGINEERING
IJTE
ISSN: 2057-5688

of beam intensity on the deposited dosage. Consequently, the estimated

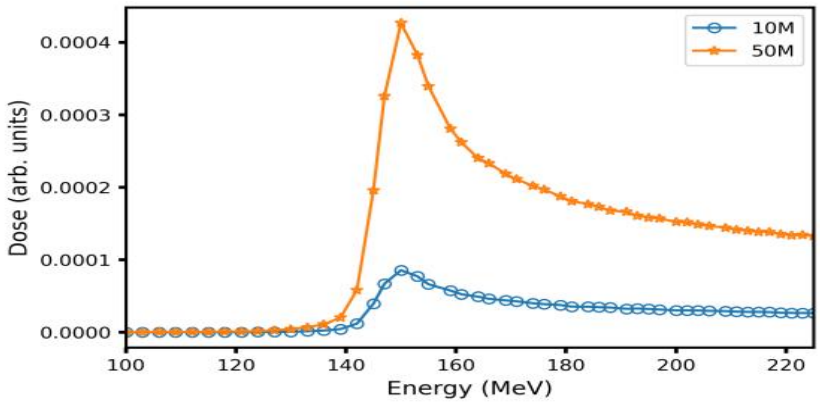

Figure 10 shows ERDFs for 150 mm using simulated beam intensities of 107 particles and 5 107 particles.

For the same WEPL, the values of the area under the curve at various beam intensities will vary. To reverse this impact, a good normalisation is necessary.

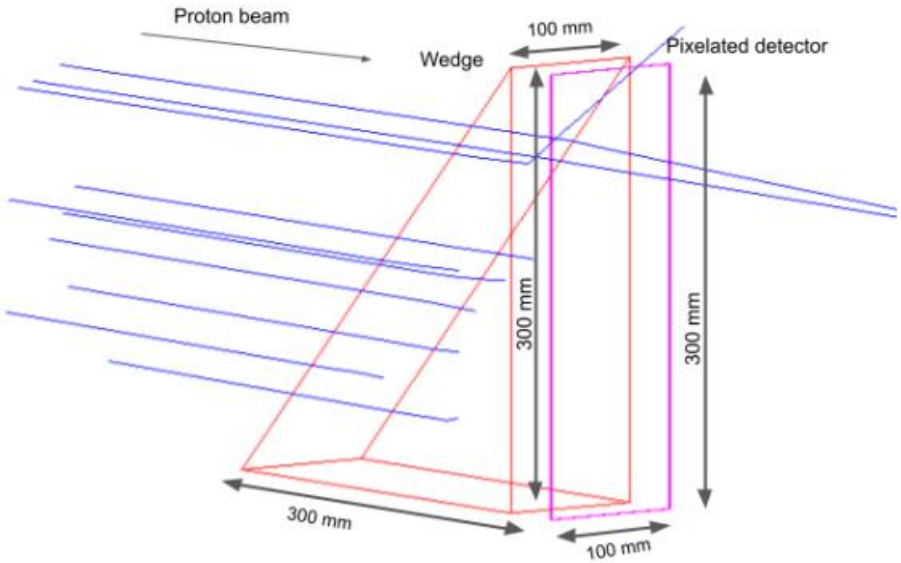

Figure 11: shows the simulation configuration in GATE that was used to produce the calibration library.

The simulation is run again with 5 107 particles to confirm the impacts of beam intensity. Additionally, the simulation is run with 107 particles

INTERNATIONAL JOURNAL OF TECHNO-ENGINEERING
IJTE
ISSN: 2057-5688

and the wedge shape is changed with individual box and stair structures. Each configuration's associated data is recorded individually. The diagrammatic depiction of the simulation's box and stair arrangements.

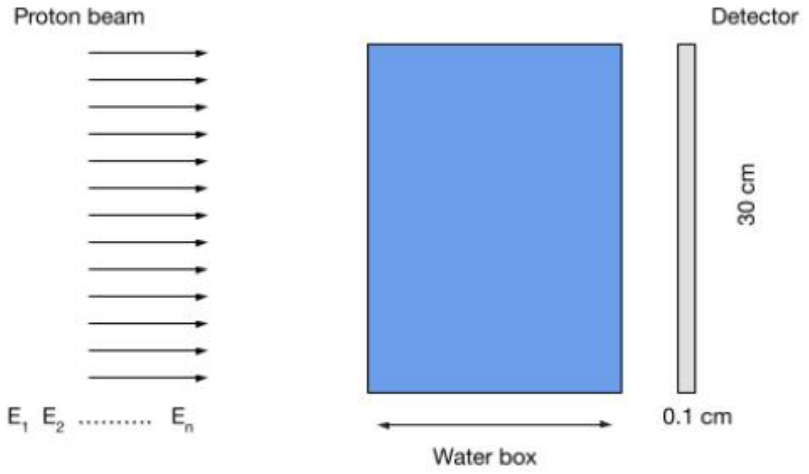

(a)

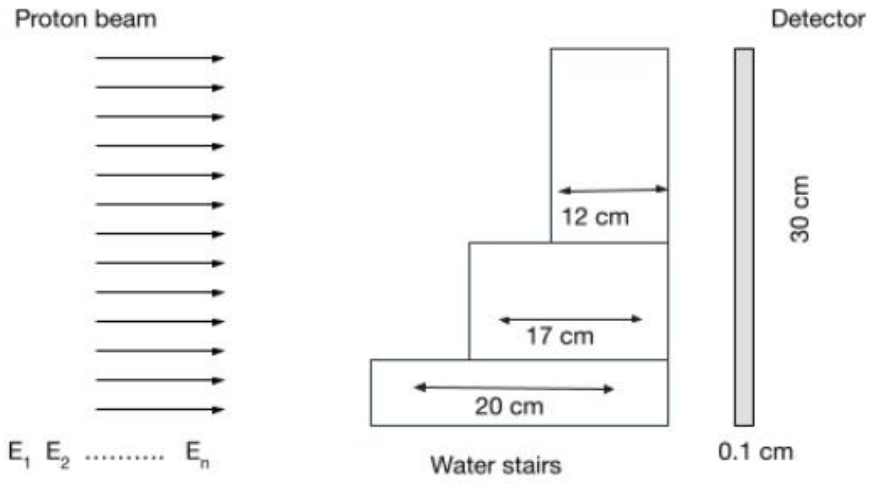

(b)

Figure 12: Schematic illustration of the GATE simulation's water box (a) and stair layout (b).

The two water box designs are known as B1 (with a thickness of 12 cm) and B2 (with a thickness of 17 cm), while the two and three-stair versions are

INTERNATIONAL JOURNAL OF TECHNO-ENGINEERING
IJTE
ISSN: 2057-5688

known as S1 and S2, respectively. Table 1 provides the dimensions of the stair layouts employed in the simulation. The GATE simulation was used to produce all of the datasets needed for our studies [17].

In the last section of our research, we looked at how the number of energy levels affected our ability to estimate the Sw parameter. The simulation research used a total of 47 energy layers and evaluated the Sw parameter. To estimate the Sw parameter, the energy layers are chosen sequentially in increments of 2, 3, and 4. The relationship between Sw and WEPL is modelled using a polynomial of order 6, which was shown to be the best match when 47 energy layers were utilised. the polynomial coefficients discovered by employing several energy layers to relate Sw and WEPL. It has been noted that the coefficients derived for the various energy layers vary.

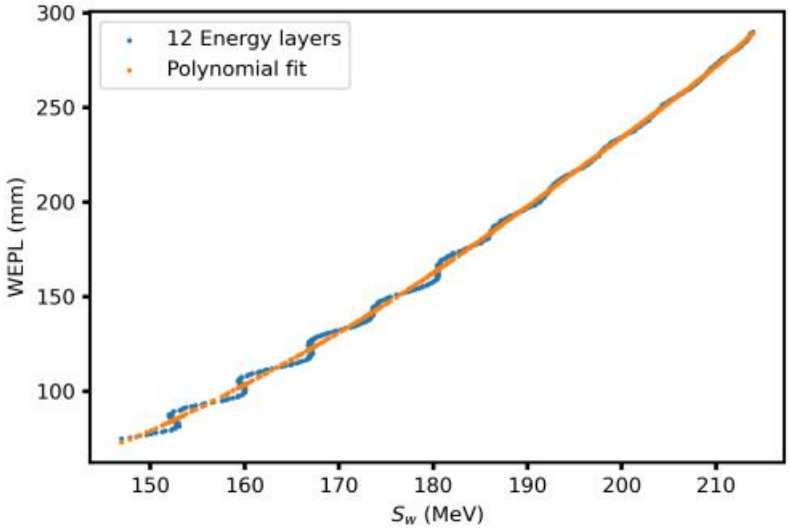

Figure 12 shows the variation of WEPL for 12 energy layers with a 6th order polynomial fit as a function of Sw.

Sw and WEPL are related using 12 energy layers and a polynomial fit of sixth order. Compared to the curve derived utilising all of the energy layers, the plot has a crinkled character. As a result, the polynomial coefficients vary depending on the employed energy layers. The findings unmistakably show that the Sw parameter is sensitive to the number of

INTERNATIONAL JOURNAL OF TECHNO-ENGINEERING
IJTE
ISSN: 2057-5688

energy layers used and also influences the precision of WEPL estimate.

V Conclusion

An innovative replacement for the 2 -minimization approach is the analytical formula for determining WEPL from the Sw parameter. Using a polynomial equation of order 6 for WEPLs greater than 75 mm, we have established a one-to-one link between Sw and WEPL in this study. According to the box configuration findings, there is a 2.5 mm standard deviation between the real and calculated WEPL distributions. The protons scattering away from the beam direction causes the greatest divergence at the margins to reach 10 mm. It was evident from the stair arrangement findings that range-mixed locations, where there is a variance in WEPL of up to 30 mm, had an impact on WEPL estimate. The general formula was unable to address the impact of range mixing at the intersection of various material thicknesses. The standard deviation for the stair layouts in the current study was around 2.7 mm, and the analysis was conducted by filtering out the range-mixed pixels. Additionally, it was discovered that the Sw parameter is sensitive to the energy layers used and that the link between Sw and WEPL deteriorates when the energy layers are reduced. This work, however, demonstrates the possibility of WEPL estimation employing a single equation with decreased computing time in picture production, which is ten times quicker than the 2 -minimisation approach. The findings indicate that more research is required in order to enhance the formula and polynomial fit. To increase the precision of the WEPL estimate, one method may be to better optimise the polynomial equation's coefficients. To address the density changes in real-world circumstances, the research must be conducted in a heterogeneous medium to assess the amount of the range mixing effect.

VI References

[1] H. Paganetti, “Range uncertainties in proton therapy and the role of Monte Carlo simulations,” Physics in Medicine and Biology, vol. 57, no. 11, 2012, doi: 10.1088/0031-9155/57/11/R99.

[2] A. C. Knopf and A. Lomax, “In vivo proton range verification: A

INTERNATIONAL JOURNAL OF TECHNO-ENGINEERING
IJTE
ISSN: 2057-5688

review," Physics in Medicine and Biology, vol. 58, no. 15, pp. 131–160, 2013, doi: 10.1088/0031-9155/58/15/R131.

[3] J. Unkelbach, T. C. Y. Chan, and T. Bortfeld, "Accounting for range uncertainties in the optimization of intensity modulated proton therapy," Physics in Medicine and Biology, vol. 52, no. 10, pp. 2755–2773, 2007, doi: 10.1088/0031-9155/52/10/009.

[4] K. Parodi and J. C. Polf, "In vivo range verification in particle therapy," Medical Physics, vol. 45, no. 11, pp. e1036–e1050, 2018, doi: 10.1002/mp.12960.

[5] A. Fredriksson, A. Forsgren, and B. Hårdemark, "Minimax optimization for handling range and setup uncertainties in proton therapy," Medical Physics, vol. 38, no. 3, pp.1672–1684, 2011, doi: 10.1118/1.3556559.

[6] M. Mumot, C. Algranati, M. Hartmann, J. M. Schippers, E. Hug, and A. J. Lomax,"Proton range verification using a range probe: Definition of concept and initial analysis," Physics in Medicine and Biology, vol. 55, no. 16, pp. 4771–4782, 2010, doi:10.1088/0031-9155/55/16/010.

[7] W. D. Newhauser and R. Zhang, "The physics of proton therapy," Physics in Medicine and Biology, vol. 60, no. 8, pp. R155–R209, 2015, doi: 10.1088/0031-9155/60/8/R155.

[8] P. Farace, R. Righetto, S. Deffet, A. Meijers, and F. vander Stappen, "Technical Note:A direct ray-tracing method to compute integral depth dose in pencil beam proton radiography with a multilayer ionization chamber," Medical Physics, vol. 43, no. 12,pp. 6405–6412, 2016, doi: 10.1118/1.4966703.

[9] P. Farace, R. Righetto, and A. Meijers, "Pencil beam proton radiography using a multilayer ionization chamber," Physics in Medicine and Biology, vol. 61, no. 11, pp.4078–4087, 2016, doi: 10.1088/0031-9155/61/11/4078.

[10] A. Hammi, S. Koenig, D. C. Weber, B. Poppe, and A. J. Lomax, "Patient positioning verification for proton therapy using proton radiography," Physics in Medicine andBiology, vol. 63, no. 24, 2018, doi: 10.1088/1361-6560/aadf79.

INTERNATIONAL JOURNAL OF TECHNO-ENGINEERING
IJTE
ISSN: 2057-5688

[11] A. Hammi, L. Placidi, D. C. Weber, and A. J. Lomax, "Positioning of head and neck patients for proton therapy using proton range probes: A proof of concept study," Physics in Medicine and Biology, vol. 63, no. 1, 2018, doi: 10.1088/1361-6560/aa9cff.

[12] S. Deffet, B. Macq, R. Righetto, F. vander Stappen, and P. Farace, "Registration ofpencil beam proton radiography data with X-ray CT," Medical Physics, vol. 44, no. 10, pp. 5393–5401, 2017, doi: 10.1002/mp. 12497.

[13] U. Schneider, P. Pemler, J. Besserer, E. Pedroni, A. Lomax, and B. Kaser-Hotz, "Patient specific optimization of the relation between CT-Hounsfield units and proton stopping power with proton radiography," Medical Physics, vol. 32, no. 1, pp. 195–199, 2005, doi: 10.1118/1.1833041.

[14] U. Schneider and E. Pedroni, "Proton radiography as a tool for quality control in proton therapy," Medical Physics, vol. 22, no. 4, pp. 353–363, 1994, [Online]. Available: https://doi.org/10.1118/1.597470

[15] P. J. Doolan, M. Testa, G. Sharp, E. H. Bentefour, G. Royle, and H. M. Lu, "Patient-specific stopping power calibration for proton therapy planning based on single-detector proton radiography," Physics in Medicine and Biology, vol. 60, no. 5, pp.1901–1917, 2015, doi: 10.1088/0031-9155/60/5/1 901.

[16] K. H. Cha, L. Hadjiiski, R. K. Samala, H. P. Chan, E. M. Caoili, and R. H. Cohan,"Urinary bladder segme ntation in CT urography using deep-learning convolutional neural network and level sets," Medical Physics, vol. 43, no. 4, pp. 1882–1886, 2016, doi: 10.1118/1.4944498.

[17] K. H. Jin, M. T. Mccann, E. Froustey, and M. Unser, "Deep Convolutional Neural Network for Inverse Problems in Imaging," in IEEE transactions on image processing, 2017, vol. 26, no. 9, pp. 4509–4522.

[18] A. Thummerer et al., "Comp arison of CBCT based synthetic CT methods suitable for proton dose calculations in adaptive proton therapy," Physics in Medicine & Biology, 2020, doi: 10.1088/1361-6560/ab7d54.

[19] D. Nguyen et al., "A feasibility study for predicting optimal radiation therapy dose distributions of prostate cancer patients from patient anatomy

INTERNATIONAL JOURNAL OF TECHNO-ENGINEERING
IJTE
ISSN: 2057-5688

using deep learning," Scientific Reports, vol. 9, no. 1, pp. 1–10, 2019, doi: 10.1038/s41598-018-37741-x.

019, doi: 10.1002/mp.13264.

[20] B. Sahiner et al., "Deep learning in medical imaging and radiation therapy," Medical Physics, vol. 46, no. 1, pp. e1–e36, 2